

Baryon Resonance Extraction from πN Data using a Multichannel Unitary Model

S.A. Dytman and T.P. Vrana

Dept. of Physics and Astronomy, University of Pittsburgh, Pittsburgh, PA 15260

T.-S. H. Lee

Physics Division, Argonne National Laboratory, Argonne, IL 60439

We present organization and solutions for a new analysis of all πN elastic and the major inelastic channels to extract detailed characteristics of the contributing baryon resonances. This work is based on the work of R. Cutkosky and collaborators at CMU about 20 years ago. The model features analyticity at the amplitude level and unitarity. Results are similar to previous analyses for strongly excited states, but can vary considerably from previous analyses when the states are weak, the data is poor, or there is a strong model dependence. We emphasize the $S_{11}(1535)$ resonance which has particularly strong model dependence.

1 Introduction

A primary goal in analyzing pion-nucleon elastic and inelastic data is to ascertain the underlying resonant structure. The properties of the N^* resonances are an important window into the behavior of strongly interacting systems at large distance (~ 1 fm). Many inelastic channels contribute roughly equally to the total πN total cross section. A correct analysis should account for all of them in establishing unitarity, matching all available data, and including the proper threshold characteristics.

The data must be decomposed into partial waves and separated into the various resonance contributions and their asymptotic channel excitation widths (e.g. the partial decay width into πN , ηN , γN , ωN , ρN , $\pi\Delta$, $\pi N^*(1440)$, and others) before the model calculations can be compared to data. In the resonance region, the threshold effects of asymptotic channels must be handled correctly to ensure a proper identification of resonances. This is particularly important for the $S_{11}(1535)$ where the ηN threshold comes just below the resonance pole position.

Resonance extraction requires a significant calculational effort and many articles have presented various ways to determine resonance parameters (masses, pole positions, and decay widths) from data. The PDG mostly bases its recommendations on older work by Cutkosky et al. (the Carnegie-Mellon Berkeley or CMB group)¹ and Höhler et al. (the Karlsruhe-Helsinki or KH group)², and more recent work by Manley and Saleski (or KSU)³ and the VPI group.⁴ All these efforts use reaction data with πN initial states. All maintain unitarity, though the methods employed are quite different. These models handle the multichannel character of the reactions

in quite different ways. CMB and KSU use a formalism that allows for many channels while KH and VPI focus on the πN elastic channel by including a dummy channel to account for all inelasticity. For most strongly excited states, the four analyses tend to agree within expected errors on resonance masses and widths. A notable exception is $S_{11}(1535)$ where extracted full widths are 66 MeV^4 , $120 \pm 20 \text{ MeV}^2$, $151 \pm 27 \text{ MeV}^3$, and $270 \pm 50 \text{ MeV}^1$. This large variation is due to the close proximity of the resonance pole to the ηN threshold.

This work presented here applies the CMB model¹ to πN data with a large variety of final states. This model emphasizes the proper treatment of all analytic features that might be found in the complex energy plane. The main publication where the CMB model was used was published in 1979. Although they used both elastic and inelastic data, the elastic data was emphasized. Significant analysis was required⁵ in order to represent the data in a model independent form.

Batinic et al.⁶ have applied the CMB model to more recent data including three channels (πN , ηN , and a dummy channel meant to represent $\pi\pi N$). They use the KH80 model independent analysis of the πN elastic data and the $\pi N \rightarrow \eta N$ data to produce a new fit to the S_{11} channel. They determine a full width of the $S_{11}(1535)$ to be 151 MeV .

We present a minimal account of the model and show the model dependence for the analysis of the data discussed above. In this paper, we discuss some representative results. We will provide a more complete list of baryon resonances and description of the model in a forthcoming paper⁷.

2 Features of the Model

The CMB model seeks a representation of the scattering T matrices for many channels combining desirable properties of analyticity and unitarity. The phase space factors $\phi(s)$ (called the channel propagators in the original paper) are calculated with a dispersion relation which guarantees analyticity in the solutions. This makes the search for the actual pole of the T matrix in complex s space possible. Self energies are calculated for the coupling of each resonance to asymptotic states as it propagates and are included via a Dyson equation. Since there are multiple open channels, we use the matrix form of the Dyson equation to calculate the full resonance propagator G. The self energies provide the required dressing of the bare states to produce the physical states seen in experiments. Final states of two pions and a nucleon are included in the phase space factors as quasi-two-body states with an appropriate width.

A separable form for the T matrix is assumed. Although this form most easily allows reproduction of s-channel processes, additional nonresonant processes are included in background.

We have reproduced the CMB model¹ and present fits to modern data sets. The same form factors and dispersion relations are used. Eight asymptotic channels are

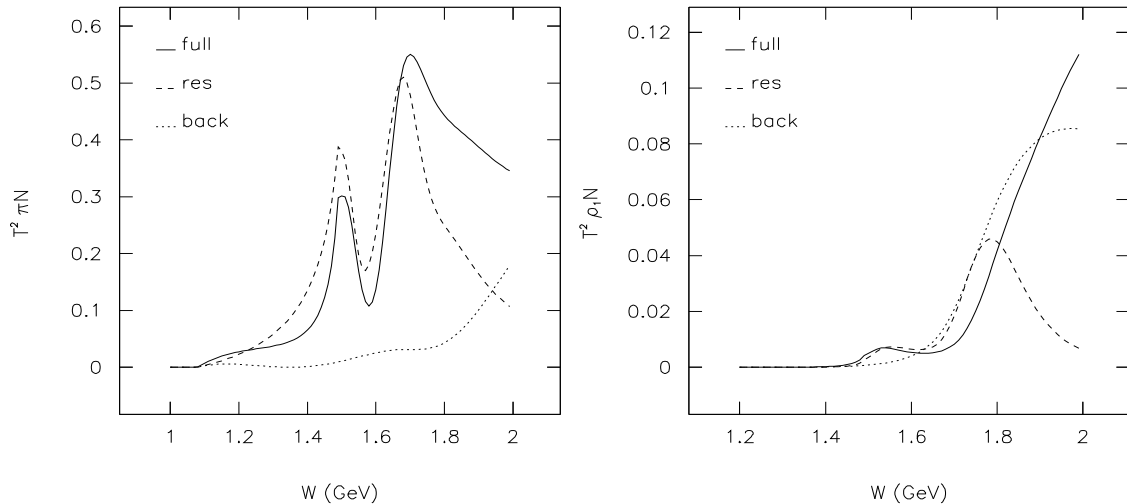


Figure 1: Resonance-Background Separation for the πN and ρN channels in the S_{11} partial wave

allowed to couple to the resonances in each partial wave. Two or three nonresonant terms are included in each partial wave. These are represented as resonances at energies well below or well above the resonance region. Lacking a specific model for these processes, they have the same bare energy dependence (smooth) used for resonances, but the inelastic thresholds produce the appropriate analytic behavior for each nonresonant term. We show the separation of resonant and nonresonant parts for the magnitude of the T matrix element for elastic scattering and ρ production in Figure 1.

3 Model Dependence in the S_{11} Partial Wave

The variation between this and other models can best be seen in an analysis of the data in the $\pi N S_{11}$ channel. Here, there are 2 strong resonances that have unusual features that are difficult to describe. The $S_{11}(1535)$ has the ηN threshold close to the peak of the resonance and the two states have significant overlap. Data for both the $\pi N \rightarrow \pi N$ and $\pi N \rightarrow \eta N$ would be required for a high quality fit. Presently, data for eta production is of much less quality than for the elastic channel.

We have analyzed all available data for the S_{11} channel with the full CMB model and various approximations that simulate the models employed by various other groups. Results are shown in Tables 1 and 2. Columns are labeled by the features of the model employed and the results of that model. All models are unitary, but this is done with either a K matrix treatment or the full Dyson equation. To construct the K matrix model, we use the truncated diagonal Dyson equation using just the first term. Thus, the resonance coupling to other resonances in the intermediate state is disabled. The analytic properties are turned off by setting the real part of $\phi(s)$ to

Table 1: Fitting results for the lowest energy resonance found in the S_{11} partial wave for various models. The model characteristics on the right four columns are used to make the fits with results shown in the five columns on the right. See text for details. $S_{11}(1535)$

Mass MeV	Width MeV	πN %	ηN %	$\pi\pi N$ %	Unitarity	Disp. Rel.	Res Type	Channels in fit
1518	87	43	6	51	K-Matrix	NO	NRBW	πN
1532	108	45	39	16	K-Matrix	NO	NRBW	πN , ηN
1535	126	42	44	14	K-Matrix	NO	NRBW	ALL
1514	84	35	0	65	K-Matrix	NO	RBW	πN
1533	110	44	40	16	K-Matrix	NO	RBW	πN , ηN
1534	125	42	43	15	K-Matrix	NO	RBW	ALL
1531	72	16	62	22	Dyson eq.	YES	RBW	πN
1526	114	36	41	23	Dyson eq.	YES	RBW	πN , ηN
1542	112	35	51	14	Dyson eq.	YES	RBW	ALL

zero; the imaginary part still contains the correct phase space. We also compare results obtained with a relativistic and nonrelativistic Breit-Wigner shape for the bare resonance. Finally, we used various data sets in the fit since not all published models use data from all inelastic channels.

We first note that without the dispersion relation, the T matrices for the K-matrix model and the model using the Dyson equation for the resonance propagator are equivalent. Therefore, only the K-matrix results without the dispersion relation are given in the table.

In general, the choice of relativistic vs. nonrelativistic shape for the bare Breit-Wigner resonance does not have a strong influence for an isolated resonance such as the 1535 MeV state. However, the 1650 MeV state has a weaker signal (in part because of poorer data quality) and the two shapes can produce larger differences. Even there, the case where all data is used (line 3 vs. line 6) has much less difference between RBW and NRBW.

More important differences are found when comparing K-matrix vs. Dyson results with the dispersion relation included (e.g. line 6 vs. line 9). The former is close to the model employed by Manley and Saleski. These two models have differences of about 10% in the total width and up to 50% in the branching ratios.

The most important deviation from the full result comes from the use of a truncated data set. For the 1535 MeV state, ignoring the interference with the ηN final state causes the model to fit the Breit-Wigner shape to the cusp at the ηN threshold. The VPI work has a very small width for the 1535 MeV state; although the ηN channel is mocked up, none of the actual data is used. For even the full model, leaving out the πNN final state data (such as was done by Batinic et al.⁶) produces 20%

Table 2: Same as Table 1 for the $S_{11}(1650)$ Resonance. $S_{11}(1650)$

Mass MeV	Width MeV	πN %	ηN %	$\pi\pi N$ %	Unitarity	Disp. Rel.	Res Type	Channels in fit
1645	233	35	49	16	K-Matrix	NO	NRBW	πN
1689	225	67	31	2	K-Matrix	NO	NRBW	πN , ηN
1694	259	72	16	12	K-Matrix	NO	NRBW	ALL
1682	161	78	5	17	K-Matrix	NO	RBW	πN
1692	233	75	15	10	K-Matrix	NO	RBW	πN , ηN
1690	229	65	25	10	K-Matrix	NO	RBW	ALL
1692	138	65	35	0	Dyson eq.	YES	RBW	πN
1676	104	54	45	1	Dyson eq.	YES	RBW	πN , ηN
1689	202	74	6	20	Dyson eq.	YES	RBW	ALL

deviations in the branching ratios. We reproduce the updated results of the Batinic et al. paper⁶.

4 Results and Discussion

We have applied the CMB model to the πN elastic T matrices of VPI⁴, the inelastic T matrices of Manley et al.⁸, and our own partial wave analysis of the $\pi N \rightarrow \eta N$ data (leaving out the controversial Brown et al. data⁹). At this time, the VPI analysis⁸ is the best available information about the $\pi N \rightarrow \pi\pi N$ reactions. A more objective analysis would use experimental data points rather than the “partial wave decomposed” data we use in this paper. A reanalysis of the $\pi N \rightarrow \pi\pi N$ data is in progress at the University of Pittsburgh; a more complete analysis can be presented when that is finished.

The analysis presented here is a mixture of CMB¹ and KSU³ since we use the formalism of the former and a data set similar to that used by the latter. Although the data set used here is very similar to that used by KSU, they do not include the $\pi N \rightarrow \eta N$ data and use older elastic information.

A partial list of resonances found in this analysis is given in Tables 3 and 4 and compared to the results of KSU, those of CMB and the latest recommended values given by PDG. The number of states sought in each partial wave was the same as used by KSU³. We also show figures for a few representative cases.

The number of fit parameters depends on the number of resonances to be fit and the inelastic couplings fit; for the S_{11} partial wave (see Figs. 2 and 3), there are 3 resonances and we fit to the bare pole and the couplings to 7 channels for each. There are also 2 subthreshold and 1 high energy ‘states’ used to simulate background.

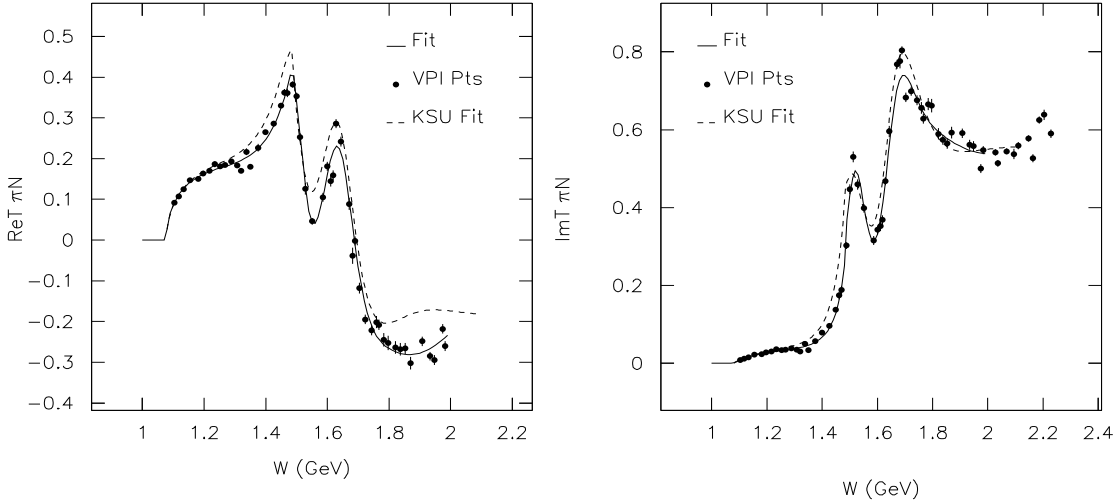


Figure 2: $S_{11} \pi N$ Elastic T-matrix Element

Three parameters, a bare resonance energy and coupling strengths to πN and ηN are fit for each background pole. Thus, there are 38 parameters fit in this partial wave. For the D_{15} partial wave (see Fig. 4), only 1 resonance (with coupling to 4 channels) and 3 background poles were fit, a total of 14 real parameters. Since the elastic data is of much higher quality than the inelastic data, the elastic data was weighted by a factor of 2 higher than the inelastic in order to ensure a reasonable fit to the elastic data. Although the elastic data could be fit well, the inelastic data was not. For elastic data, typical values of $\chi^2/datapoint$ were 1.7 and 1.6 for the S_{11} and D_{15} waves, respectively. For the inelastic amplitudes, $\chi^2/datapoint$ values were 9.2 and 22.2. Although we get better fits to the elastic data than Manley and Saleski³, the inelastic fits are of similar quality in each analysis. (No values of χ^2 are given by KSU.) However, the shapes of our inelastic T matrices are qualitatively different in many cases.

For a complicated multiparameter fit, errors are difficult to determine because correlations can be significant. A Monte Carlo sampling technique was used. Resonance poles and physical quantities are found for many values of fit parameters, chosen according to the errors derived by MINUIT. Ten thousand such searches were made for each partial wave. This method is similar to that employed by KSU and similar errors result. This error is almost entirely statistical and only uses the diagonal errors from the partial wave decompositions. No systematic sources (e.g. due to the assumption of a Breit-Wigner shape for the bare resonance) are included.

Strong isolated resonances that have a strong elastic coupling are fit well with all models. The resonance parameters for these states, e.g. the $D_{15}(1675)$ and $F_{15}(1680)$ masses and widths, tend to have close agreement between previous results and the new results.

The benefit of the multichannel analysis is readily apparent for states with a very

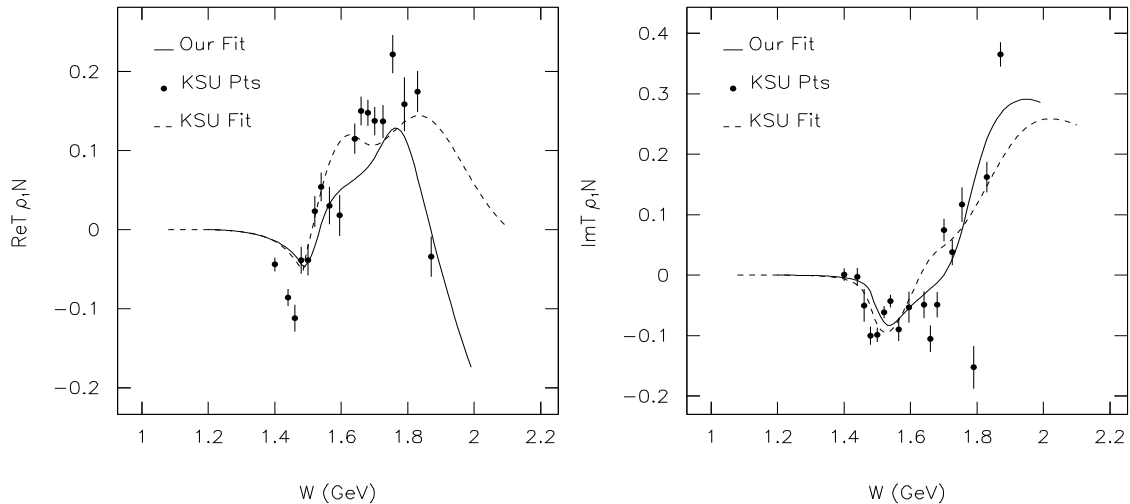


Figure 3: $S_{11} \pi N \rightarrow \rho N$ T-matrix Element

small elastic branching fraction. For example, $D_{13}(1700)$ is not seen in the VPI ⁴ elastic analysis because the only sign of the resonance in the elastic channel is a shallow dip in the real part of the T matrix. However, there is a strong resonance signal in the $\pi N \rightarrow \pi \Delta$ T matrix.

Agreement with the KSU analysis is mixed. For the cases where KSU differs significantly from the consensus of previous results, the $S_{31}(1620)$ mass and the $S_{11}(1650)$ elasticity, the new results tend to agree with the older values. Since the data sets used for the Pitt-Argonne and KSU analyses are very similar, any differences can most likely be attributed to differences in the model employed. To verify this, we redid fits with the same elastic data as used by KSU and found qualitatively similar results to those in the tables. For $F_{15}(1680)$, agreement is within errors for the largest decay branches. However, $S_{31}(1620)$ is a strong state state where agreement is not good. For the $S_{31}(1920)$, the elastic “partial wave decomposed” data has changed significantly from the set used by KSU to the set we used. The full width for KSU is 5 times larger than the new result.

5 Conclusions

We present results for a new analysis of the *best available* πN “partial wave decomposed” data. We apply a model ¹ that contains all the correct analytic properties. The results can differ significantly from previous analyses, due to either the new data sets used in this work or due to model dependence. A more complete discussion can be found in a forthcoming paper. ⁷

At present, the main limitation in any analysis is the data. Improved πN inelastic data is badly needed to generate high quality fits required for objective results.

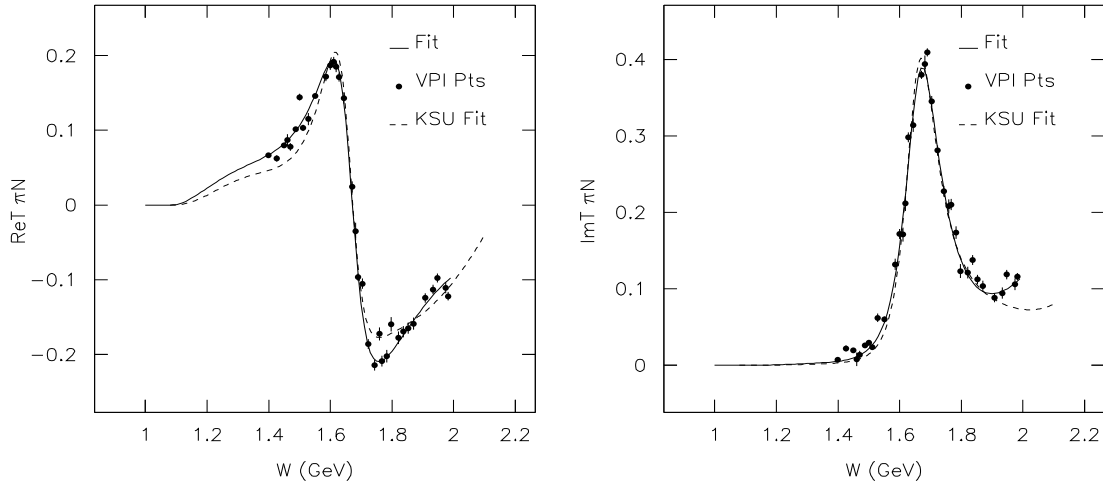


Figure 4: $D_{15} \pi N$ Elastic T-matrix Element

Acknowledgments

We are grateful to Mark Manley and Dick Arndt for providing the “partial wave decomposed” data used in this study. We also wish to thank Matt Mihalcin, Jay deMartino, and David Kokales for their significant programming contributions to this work.

1. R.E. Cutkosky, C.P. Forsyth, R.E. Hendrick, and R.L. Kelly, Phys. Rev. **D20**, 2839 (1979).
2. G. Höhler, F. Kaiser, R. Koch, and E. Pietarinen, *Handbook of Pion-Nucleon scattering*, [Physics Data No. 12-1 (1979)]
3. D.M. Manley and E.M. Saleski, Phys. Rev. **D45**, 4002 (1992).
4. Richard A. Arndt, Igor I. Strakovsky, Ron L. Workman, and Marcello M. Pavan, Phys. Rev. **C52**, 2120 (1995).
5. R. Kelly and R.E. Cutkosky, Phys. Rev. **D 20**, 2782 (1979).
6. M. Batinic, I. Slaus, A. Svarc, and B.M.K. Nefkens, Phys. Rev. **C51**, 2310 (1995), private communication.
7. T.P. Vrana, S.A. Dytman, and T.-S.H. Lee, to be published.
8. D.M. Manley, R.A. Arndt, Y. Goradia, and V.L. Teplitz, Phys. Rev. **D30**, 904 (1984).
9. R.M. Brown, et al., Nucl. Phys. **B153**, 89 (1979).

Table 3: Comparison of Resonance Masses and Widths for Selected Resonances

Resonance	Mass (MeV)	Width (MeV)	Elasticity %	Reference
S ₁₁ (1535) ****	1542(15)	112(30)	35(5)	PITT-ARG
	1534(7)	151(27)	51(5)	KSU
	1520-1555	100-250	35-55	PDG
	1550(40)	240(80)	50(10)	CMB
P ₁₁ (1440) ****	1479(9)	490(18)	72(3)	PITT-ARG
	1462(10)	391(34)	69(3)	KSU
	1430-1470	250-450	60-70	PDG
	1440(30)	340(70)	68(4)	CMB
D ₁₃ (1520) ****	1518(13)	124(25)	63(4)	PITT-ARG
	1524(4)	124(8)	59(3)	KSU
	1515-1530	110-135	50-60	PDG
	1525(10)	120(15)	58(3)	CMB
D ₁₅ (1675) ****	1685(13)	131(26)	35(4)	PITT-ARG
	1676(2)	159(7)	47(2)	KSU
	1670-1685	140-180	40-50	PDG
	1675(10)	160(20)	38(5)	CMB
F ₁₅ (1680) ****	1679(11)	128(23)	69(4)	PITT-ARG
	1684(4)	139(8)	70(3)	KSU
	1675-1690	120-140	60-70	PDG
	1680(10)	120(10)	62(5)	CMB
S ₃₁ (1620) ****	1617(10)	143(19)	45(3)	PITT-ARG
	1672(7)	154(37)	9(2)	KSU
	1615-1675	120-180	20-30	PDG
	1620(20)	140(20)	25(3)	CMB
P ₃₃ (1232) ****	1234(2)	112(3)	100(1)	PITT-ARG
	1231(1)	118(4)	100(0)	KSU
	1230-1234	115-125	98-100	PDG
	1232(3)	120(5)	100(0)	CMB

Table 4: Branching Ratios for Selected Resonances

Resonance	Channel	PITT-ARG	KSU	PDG
S ₁₁ (1535)	πN	35(5)	51(5)	35-55
	ηN	51(6)	43(6)	30-55
	$\rho_1 N$	2(6)	2(1)	0-4
	$(\rho_3 N)_D$	0(0)	1(1)	
	$(\pi \Delta)_D$	1(1)	0(0)	0-1
	$(\epsilon N)_P$	2(6)	1(1)	0-3
	$\pi N^*(1440)$	10(10)	2(2)	0-7
S ₁₁ (1650)	πN	74(3)	89(7)	55-90
	ηN	6(6)	3(5)	3-10
	$\rho_1 N$	1(3)	0(0)	4-14
	$(\rho_3 N)_D$	13(4)	3(2)	
	$(\pi \Delta)_D$	2(5)	2(1)	3-7
	$(\epsilon N)_P$	1(4)	2(2)	0-4
	$\pi N^*(1440)$	3(5)	1(1)	0-5
D ₁₅ (1675)	πN	35(4)	47(2)	40-50
	ηN	0(0)		
	$\rho_1 N$	0(8)	0(0)	1-3
	$(\rho_3 N)_D$	1(8)	0(0)	
	$(\pi \Delta)_D$	63(4)	53(2)	50-60
F ₁₅ (1680)	πN	69(4)	70(3)	60-70
	ηN	0(0)		
	$(\rho_3 N)_F$	3(2)	2(1)	1-5
	$(\rho_3 N)_P$	5(3)	5(3)	0-12
	$(\pi \Delta)_F$	1(3)	1(1)	0-2
	$(\pi \Delta)_P$	14(2)	10(3)	6-14
	$(\epsilon N)_D$	9(3)	12(3)	5-20
S ₃₁ (1620)	πN	45(3)	9(2)	20-30
	$\rho_1 N$	14(2)	25(6)	7-25
	$(\rho_3 N)_D$	2(4)	4(3)	
	$(\pi \Delta)_D$	39(2)	62(6)	30-60
	$\pi N^*(1440)$	0(6)		